Pergamon

0956-7151(94)E0102-M

*Acta metall. mater.* Vol. 42, No. 9, pp. 2943–2954, 1994

0956-7151/94 $7.00 + 0.00

# MICROSCOPIC MASTER EQUATION APPROACH TO DIFFUSIONAL TRANSFORMATIONS IN INHOMOGENEOUS SYSTEMS—SINGLE-SITE APPROXIMATION AND DIRECT EXCHANGE MECHANISM

**LONG-QING CHEN[1] and J. A. SIMMONS[2]**

[1]Department of Materials Science and Engineering, Pennsylvania State University, University Park, PA 16802 and [2]Metallurgy Division, National Institute of Standards and Technology, Gaithersburg, MD 20899, U.S.A.

*(Received 14 October 1993; in revised form 16 February 1994)*

**Abstract**—A computer simulation technique based on microscopic master equations is developed for modeling the dynamics of morphological evolution during diffusional phase transformations in binary solid solutions including barrierless nucleation of ordered domains, subsequent domain growth and coalescence, coarsening of antiphase domains, compositional phase separation, Ostwald ripening, and kinetics of simultaneous ordering and phase separation. Assuming a direct exchange mechanism for atomic diffusion and using the single-site approximation, the kinetic equations produce equilibrium states closer to the Bethe approximation than the Bragg–Williams approximation. Computer simulation examples of microstructural evolution during ordering, spinodal decomposition, and simultaneous ordering and phase separation in a binary solid solution are presented using a second-neighbor interaction model.

## INTRODUCTION

Understanding the temporal and spatial evolution of the morphology of a quenched system is not only of fundamental interest to physicists, materials scientists and applied mathematicians but is also important in the processing of technologically advanced materials. The highly nonlinear and nonequilibrium dynamics of phase transformations have been extensively studied by employing continuum Ginzburg–Landau- or Cahn–Hilliard-type kinetic equations [1]. More recently, one of us has used a microscopic kinetic model, which employs the Onsager-type microscopic diffusion equations developed by Khachaturyan in 1968 [2], for investigating the dynamics of ordering and phase separation [3], formation of virtual phases [4] and strain-induced morphological transformation during decomposition [5–6] in quenched binary alloy systems. Both the continuum and microscopic equations are based on a free energy functional which depends on inhomogeneous distribution of local order parameters in the continuum model or the single-site occupation probabilities in the microscopic model. Both approaches describe the rate change of the order parameter or occupation probabilities with respect to time as linearly proportional to the thermodynamic driving force. Therefore, in principle, the description of kinetics by these two approaches are only valid when a system is not too far from equilibrium state, i.e. the driving force for phase transformation is small. Furthermore, the proportionality constants in both the continuum and microscopic equations are assumed to be independent of the values of the local order parameter or the occupation probabilities. Therefore, even though they predict correctly the qualitative sequence of the evolution dynamics of an inhomogeneous unstable system, they might be in error in describing the quantitative rates of such transformations.

In this paper we apply a new microscopic kinetic model [7] which utilizes a general inhomogeneous cluster expansion formalism to make tractable the microscopic Master Equations as suggested for diffusional ordering by Vineyard about 30 years ago [8]. In this model, free energy functionals do not enter into the kinetic equations of motion. The kinetic equations are written with respect to one-particle cluster, two-particle cluster or $n$-particle cluster correlation functions (where $n$ is the number of particles in a given cluster), depending on the level of approximation. Rates of change of those cluster correlation functions are proportional to the exponential of an activation energy for atomic diffusion jumps. This model is called the cluster activation method [7, 9].

Cluster activation method may be used to describe the kinetics of phase transformations of a system far from equilibrium because it does not suffer from the approximation that the rate of change of an order

parameter is linearly proportional to the thermodynamic driving force. The dependency of atomic diffusion or exchange on the local atomic configuration is automatically taken into account in the evaluation of the total activation energy for a given atomic interchange. Therefore, it is a substantial improvement over the continuum and microscopic equations derived from a free energy functional in terms of describing the rate of transformation.

Recently Ducastelle [10] has shown that, in the spin-flip dynamics context, kinetic master equations are equivalent to those of the Path Probability Method (PPM) [11] which has been applied to describe homogeneous ordering kinetics in alloys [12, 13]. In cluster activation method the maximum probability assumption of PPM is replaced with the mean value of a Bernoulli probability distribution.

The earliest application of a Master-Equation-based approach to diffusional transformations in solids appears to be the work of Iida on short- and long-range order in homogeneous $Ni_3Fe$ alloys [14]. The kinetics of both short- and long-range order in $Cu_3Au$ were discussed by Roberts and Vineyard [15]. Subsequently, homogeneous short-range order kinetics in f.c.c. were studied by Kidin and Shtremel [16], Welch [17] and Radelaar [18]. More recent works include the theoretical analysis of the linearized short- and long-range order kinetic equations by Yamauchi and de Fontaine [19], discussion of short- and long-range order as well as phase separation by Van Baal [20], and the derivation of kinetic equations for homogeneous ordering in the tetrahedral approximation for b.c.c. and f.c.c. systems [21]. In a series of papers, Fultz described B2 and $D0_3$ order in binary and ternary Fe–Al alloys [22, 23]. We emphasize that virtually all previous works required translational symmetry and were concerned with homogeneous systems. They were almost exclusively devoted to order–disorder transformations as is necessitated in that context. The only exception seems to be the investigation of one-dimensional ordering and phase separation by Van Baal [24].

In this paper, we study inhomogeneous ordering and phase separation in a two-dimensional square lattice by assuming a direct exchange mechanism (Kawasaki Dynamics) and employing the single-site approximation, thereby eliminating many complex issues involving atomic clusters. The input information required for cluster activation method is the initial atomic configuration of an alloy and the effective interaction energies between atoms. It will be shown below that, using this technique, we can successfully model various kinetic phenomena including ordered domain nucleation and growth, antiphase domain coarsening, spinodal phase separation, composition domain coarsening, as well as simultaneous ordering and phase separation. It is demonstrated that the single-site approximation in the present kinetic model yields a dependence of long-range order parameter closer to the Bethe approximation than the Bragg–Williams (BW) approximation.

## MULTIPARTICLE DISTRIBUTION FUNCTIONS

Let us consider a binary alloy with two kinds of atoms, A and B, on a crystal lattice. The structural state of an alloy at a given temperature and pressure can be completely described by a set of multiparticle distribution functions or cluster probabilities [8]. Define $P_{\alpha_1,\ldots,\alpha_n}(\mathbf{r}_1,\ldots,\mathbf{r}_n;t)$ as the probability that at a given moment of time, $t$, the $n$ lattice sites, $\mathbf{r}_1,\ldots,\mathbf{r}_n$, be simultaneously occupied by $n$ atoms of type $\alpha_1,\ldots,\alpha_n$ ($\alpha$ = A or B for binary systems). These multiparticle distribution functions satisfy the following normalization conditions

$$\sum_{\alpha_1} P_{\alpha_1}(\mathbf{r}) = 1$$

$$\sum_{\alpha_2} P_{\alpha_1\alpha_2}(\mathbf{r}_1,\mathbf{r}_2) = P_{\alpha_1}(\mathbf{r}_1)$$

$$\sum_{\alpha_1} P_{\alpha_1\alpha_2}(\mathbf{r}_1\mathbf{r}_2) = P_{\alpha_2}(\mathbf{r}_2), \text{ etc.} \tag{1}$$

Summing the single-site distribution function over all lattice sites in the crystal gives

$$\sum_{\mathbf{r}} P_{\alpha}(\mathbf{r}) = N_{\alpha}$$

where $N_\alpha$ is the total number of $\alpha$-type atoms in the crystal.

## THE KINETIC EQUATIONS

Away from equilibrium all of the multiparticle distribution functions will change with time as the atomic exchange takes place on the lattice. Many different diffusion mechanisms are possible, but we will assume a direct exchange mechanism and an isothermal environment to make the discussion simple.

Let us consider a pair of interchange sites at $\mathbf{r}$ and a nearest-neighbor site, $\mathbf{r}+\delta$, and a set $\{\mathbf{x}\}$ of nearby influence sites which can affect the interchange reaction. If we have an A atom at $\mathbf{r}$, a B atom at $\mathbf{r}+\delta$, and a set of atoms $\{X\}$ at $\{\mathbf{x}\}$, we denote by $R_{AB}(\{X\})$ the rate at which the AB pair interchanges under the influence of the set of neighboring atoms $\{X\}$. Similarly, $R_{BA}(\{X\})$ is the rate at which the BA pair will interchange under the same environment when the B atom is at $\mathbf{r}$, and the A atom is at $\mathbf{r}+\delta$. Then the rate of change of the probability that the site $\mathbf{r}$ be occupied by an A atom is given by

$$\frac{dP_A(\mathbf{r})}{dt} = \sum_{\delta}\sum_{\{X\}} P_{BA\{X\}}(\mathbf{r},\mathbf{r}+\delta,\{\mathbf{x}\})R_{BA}(\{X\}) - \sum_{\delta}\sum_{\{X\}} P_{AB\{X\}}(\mathbf{r},\mathbf{r}+\delta,\{\mathbf{x}\})R_{AB}(\{X\}) \tag{2}$$

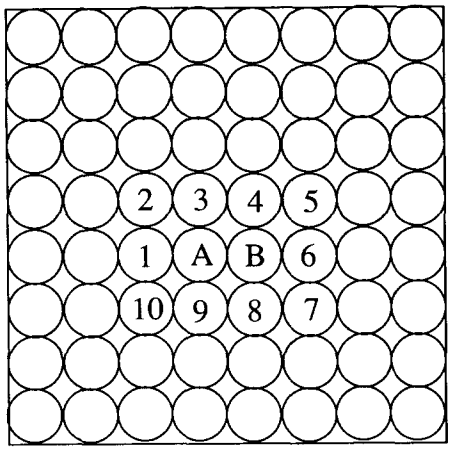


Fig. 1. A schematic draw showing the AB pair and the surrounding atoms which are affected by the pair interchange in a two-neighbor interaction model.

where the first and second terms on the right-hand side are the average rates at which, on site $\mathbf{r}$, A atoms are appearing and disappearing, respectively, $\Sigma_\delta$ denotes the summation over all the nearest neighbor sites, $\delta$, of $\mathbf{r}$, and $P_{AB\{X\}}(\mathbf{r},\mathbf{r}+\delta,\{\mathbf{x}\})$ is the probability of finding an A atom on $\mathbf{r}$, a B atom on $\mathbf{r}+\delta$, and the set $\{X\}$ on the neighboring sites $\{\mathbf{x}\}$ simultaneously. A similar equation can be written down for $dP_B(\mathbf{r})/dt$ which is simply the negative of $dP_A(\mathbf{r})/dt$ since $P_A(\mathbf{r})+P_B(\mathbf{r})=1$.

In order to carry out the sum in the right-hand side of equation (2), we need the joint probability distribution, $P_{AB\{X\}}(\mathbf{r},\mathbf{r}+\delta,\{\mathbf{x}\})$. In this paper, we use the simplest way to approximate this joint distribution by assuming statistical independence among occupation probabilities. In this approximation

$$P_{AB\{X\}}(\mathbf{r},\mathbf{r}+\delta,\{\mathbf{x}\}) = P_A(\mathbf{r})P_B(\mathbf{r}+\delta)P_{X_1}(\mathbf{x}_1)P_{X_2}(\mathbf{x}_2)\ldots P_{X_n}(\mathbf{x}_n) \quad (3)$$

where $\mathbf{x}_1,\ldots,\mathbf{x}_n$ are the individual sites in the set of neighboring sites around the pair, $\mathbf{r}$ and $\mathbf{r}+\delta$, and $X_1,\ldots,X_n$ are the types of atoms occupying those sites.

## THE RATE CONSTANTS

To calculate the reaction rates under the exchange mechanism we need only be concerned with AB interchanges, since AA and BB interchanges do not affect the atomic configuration. For a two-dimensional square lattice with a two-neighbor interaction model, we have to consider an atomic cluster of total 12 sites with an AB interchange pair surrounded by the influence set, $X$ as shown in Fig. 1. In the pairwise interaction model, we may represent the activation energy associated with the interchange pair as the sum of contributions from each of the nearest-neighbor and next-nearest neighbor sites of the pair

$$\ln R_{AB}\{X\} = \ln \nu - \sum_{i=1}^{10} \frac{U(AB,X_i)}{kT} \quad (4)$$

where $\nu$ is the vibrational frequency associated with the AB interchange and $U(AB,X_i)$ is the contribution to the activation energy from site $i$ occupied by atom $X$. Expression (4) is a form of the cluster activation approximation [7].

Symmetry considerations show that nearest neighbor and next-nearest neighbor sites, which are related by the horizontal mirror plane through the cluster center, have equivalent effects on the activation process, i.e.

$$U(AB,X_i) = U(AB,X_j)\ (i,j) \text{ or}$$

$$(j,i) = (2,10);\ (3,9);\ (4,8);\ \text{or}\ (5,7).$$

For example, an A atom occupying site 2 will make the same amount of contribution to the total activation energy for the AB pair interchange as an A atom at site 10.

Using similar symmetry arguments, we have that for the sites which are related by the vertical mirror plane through the cluster center, which is affected by the atomic interchange

$$U(AB,X_i) = U(BA,X_j)\ (i,j) \text{ or}$$

$$(j,i) = (1,6);(2,5);(3,4);(7,10);\ \text{or}\ (8,9).$$

For example, an A atom occupying site 1 will make the same contribution to the AB pair interchange as an A atom at site 6 will make to the BA pair interchange.

Accordingly, for any vertical mirror plane symmetry-related pair of indices, $i$ and $j$, we define the symmetric activation contribution, $Q$, as

$$Q(AB,X_i) = Q(AB,X_j) = \frac{1}{2}[U(AB,X_i) + U(AB,X_j)] = Q(BA,X_i) = Q(BA,X_j), \quad (5)$$

and the antisymmetric activation contribution, $E$, as

$$E(AB,X_i) = \frac{1}{2}[U(AB,X_i) - U(AB,X_j)] = -E(AB,X_j) \quad (6)$$

where $(i,j) = (1,6);(2,5);(3,4);(7,10);(8,9)$.

Therefore

$$\ln R_{AB}\{X\} = \ln \nu - \sum_{i=1}^{10} \frac{Q(AB,X_i) + E(AB,X_i)}{kT} = \ln \nu - \sum_{i=1}^{10} \frac{Q(AB,X_i)}{kT} - \sum_{i=1}^{10} \frac{E(AB,X_i)}{kT}. \quad (7)$$

$Q(\mathrm{AB},X) = \Sigma_{i=1}^{10} Q(\mathrm{AB},X_i)$ can be understood as an interdiffusion activation energy for AB interchange in an atmosphere of atoms of type $X$. Thus, the $Q$'s represent background activation energy contributions from symmetrically equivalent sites while the $E$'s give the more inhomogeneous dependence of the activation energy on local atomic configurations.

We now separate $U(AB,X_i)$ into two contributions: one is the energy of breaking bonds between $X_i$ and A or $X_i$ and B and the other is the energy of the AB complex at the activated position. For example, for an atom A at point 1, we write

$$U(\mathrm{AB},\mathrm{A}_1) = V^1_{\mathrm{AA}} = V^*_{\mathrm{AB}}$$

and for an A atom at point 6, we have

$$U(\mathrm{AB},\mathrm{A}_6) = V^1_{\mathrm{AB}} + V^*_{\mathrm{AB}}$$

where $V^1_{\mathrm{AA}}$ and $V^1_{\mathrm{AB}}$ are the first-neighbor bond energies between two A atoms and between an A atom and a B atom respectively, and $V^*_{\mathrm{AB}}$ is the contribution of each influence site to the total energy of the AB complex at the activated position. For example, the expressions for $Q$ and $E$ at site 1 and 6 when both of them are occupied by A atoms are

$$Q(\mathrm{AB},\mathrm{A}_1) = Q(\mathrm{AB},\mathrm{A}_6) = \frac{V^1_{\mathrm{AA}} + V^1_{\mathrm{AB}}}{2} + V^*_{\mathrm{AB}}$$

and

$$E(\mathrm{AB},\mathrm{A}_1) = \frac{V^1_{\mathrm{AA}} - V^1_{\mathrm{AB}}}{2}$$

$$E(\mathrm{AB},\mathrm{A}_6) = \frac{V^1_{\mathrm{AB}} - V^1_{\mathrm{AA}}}{2}.$$

Both

$$\sum_{i=1}^{10} \frac{Q(\mathrm{AB},X_i)}{kT}$$

and

$$\sum_{i=1}^{10} \frac{E(\mathrm{AB},X_i)}{kT}$$

depend on the local atomic configuration.

However, if $V^1_{\mathrm{AA}} = V^1_{\mathrm{BB}}$ and $V^2_{\mathrm{AA}} = V^2_{\mathrm{BB}}$, where $V^2_{\mathrm{AA}}$ and $V^2_{\mathrm{BB}}$ are second-neighbor bond energies between two A atoms and between two B atoms,

$$\sum_{i=1}^{10} \frac{Q(\mathrm{AB},X_i)}{kT}$$

does not depend on which type of atoms occupy the influence sites, $\{\mathbf{x}\}$. In Vineyard's treatment

$$\sum_{i=1}^{10} \frac{Q(\mathrm{AB},X_i)}{kT}$$

is set to be equal to a constant, $U_0$, which is independent of local atomic arrangement, $X$, regardless of the relative magnitudes of $V_{\mathrm{AA}}$ and $V_{\mathrm{BB}}$. In the following computer simulations, we chose $V^1_{\mathrm{AA}} = V^1_{\mathrm{BB}}$ and $V^2_{\mathrm{AA}} = V^2_{\mathrm{BB}}$, so that the rate constant takes a form equivalent to that given by Vineyard

$$R_{\mathrm{AB}}\{X\} = \nu \exp\left(-\frac{U_0}{kT}\right)\exp\left(-\sum_{i=1}^{10} \frac{E(AB,X_i)}{kT}\right). \quad (8)$$

Since $\nu \exp(-U_0/kT)$ occurs in all configurations, it can be combined with the time, $t$, in the kinetic equations of motion to give a dimensionless reduced time, $t^*$

$$t^* = t\nu \exp\left(-\frac{U_0}{kT}\right) \quad (9)$$

which will be used in the computer simulation results presented below.

Examination of the possible antisymmetric, $E$, values that can arise from any assignment easily shows that they depend only on first- and second-neighbor interchange energies, $\epsilon_1$ and $\epsilon_2$, which are given by

$$\epsilon_1 = V^1_{\mathrm{AA}} + V^1_{\mathrm{BB}} - 2V^1_{\mathrm{AB}}$$
$$\epsilon_2 = V^2_{\mathrm{AA}} + V^2_{\mathrm{BB}} - 2V^2_{\mathrm{AB}}.$$

## COMPUTER SIMULATIONS

To illustrate the application of the microscopic cluster activation method to various diffusional phase transformation kinetics we have chosen, as discussed above, a binary alloy on a two-dimensional square lattice with first- and second-neighbor pairwise interaction.

Since the summation on the right-hand side of equation (2) is over all possible arrangements of A and B atoms on the sites which are affected by the atomic interchange at $\mathbf{r}$ and $\mathbf{r}+\delta$, there are a total number of $2^{10}$ possible terms in the summation. For each of the $2^{10}$ different configurations, the rate constants $R_{\mathrm{AB}}$ and $R_{\mathrm{BA}}$ have to be calculated. The number of configurations will increase dramatically if a longer range interaction model is employed. However, in the single-site approximation, the tedious and computationally slow summation with respect to the configurations, $\{X\}$, can be replaced by a much more computationally efficient product of sums, i.e.

$$\sum_{\{X\}} P_{AB\{X\}}(\mathbf{r},\mathbf{r}+\delta,\{\mathbf{x}\})\,R_{AB}(\{X\}) = P_A(\mathbf{r})\,P_B(\mathbf{r}+\delta)$$

$$\left\{P_A(1)\exp\left[-\frac{(V^1_{AB}-V^1_{AA})}{2kT}\right]+P_B(1)\exp\left[-\frac{(V^1_{BB}-V^1_{BA})}{2kT}\right]\right\}$$

$$\left\{P_A(2)\exp\left[-\frac{(V^2_{AB}-V^2_{AA})}{2kT}\right]+P_B(2)\exp\left[-\frac{(V^2_{BB}-V^2_{BA})}{2kT}\right]\right\}$$

$$\cdots$$

$$\left\{P_A(9)\exp\left[-\frac{(V^1_{AB}-V^1_{AA})}{2kT}\right]+P_B(9)\exp\left[-\frac{(V^1_{BB}-V^1_{BA})}{2kT}\right]\right\}$$

$$\left\{P_A(10)\exp\left[-\frac{(V^2_{AB}-V^2_{AA})}{2kT}\right]+P_B(10)\exp\left[-\frac{(V^2_{BB}-V^2_{BA})}{2kT}\right]\right\} \tag{10}$$

where $P_A(k)$ and $P_B(k)$, $k = 1,10$, are the values of single-site distribution functions $P_A$ and $P_B$ at site $k$ around the pair $\mathbf{r}$ and $\mathbf{r}+\delta$.

To solve the kinetic equations, we apply the simple Euler technique

$$P_A(\mathbf{r},t+\Delta t) = P_A(\mathbf{r},t)+\frac{dP_A(\mathbf{r})}{dt}\Delta t. \tag{11}$$

## APPLICATIONS

### *Ordering*

In this case, only nearest neighbor interaction is assumed with the bond energy values given by

$$V^1_{AA} = 1.0, V^1_{BB} = 1.0, V^1_{AB} = 0.5. \tag{12}$$

Since the effective interchange energy $\epsilon_1 = V^1_{AA} + V^1_{BB} - 2V^1_{AB} = 1.0 > 0$, ordering is expected for a quenched disordered state below the ordering transition temperature. The time step in equation (11) is chosen that the numerical solution to the kinetic equation is stable. In the present case, a value of 0.1 for $\Delta t$ is chosen. The initial state at $t^* = 0$ is generated for a completely disordered state with single-site distribution function values, $P_A(\mathbf{r})$, equal to $0.5+\zeta(\mathbf{r})$ where $\zeta(\mathbf{r})$ is a random noise between $-0.01$ and 0.01. The aging temperature is 0.5 $(\epsilon_1/k)$.

The evolution of the single-site distribution function is shown in Fig. 2 for a computational cell of $32 \times 32$ lattice sites. The different gray levels represent values of the single-site distribution function at each lattice site. A completely black circle represents a value of 1 and completely white circle represents a value of 0. Shown in Fig. 2(a) is the initial disordered state where values of the single-site distribution function at each lattice site are close to the average composition $c = 0.5$. The barrierless homogeneous nucleation and subsequent growth of ordered domains are shown in Fig. 2(b) which is a snapshot of the instantaneous single-site distribution function at reduced time $t^* = 1.5$. A single-phase ordered state with antiphase domain boundaries is formed at reduced time $t^* = 2.0$ as shown in Fig. 2(c). The morphological evolution following ordering is antiphase domain coalescence and coarsening resulting in the single domain state shown in Fig. 2(d).

Figure 3 shows the evolution of the long-range order parameter values squared with the same initial condition but with a larger computational cell of $256 \times 256$ lattice sites. The long-range order parameter is calculated from the single-site distribution functions through

$$\eta(\mathbf{r}) = \frac{1}{4}\left[\sum_d P_A(\mathbf{r}+d) - 4P_A(\mathbf{r})\right](-1)^{(l+m)} \tag{13}$$

where $l$ and $m$ define the lattice vector $\mathbf{r} = a_0(l\mathbf{i}+m\mathbf{j})$, $a_0$ is the lattice parameter of the square lattice, and $\mathbf{i}$ and $\mathbf{j}$ are the unit vectors along the two Cartesian axes in two-dimensional space. The definition of long-range order parameter by expression (13) eliminates the necessity of sublattice assignment. The values of $[\eta(\mathbf{r})]^2$ is represented by different gray-levels. Bright regions are ordered regions with $[\eta(\mathbf{r})]^2$ close to 1.0 and dark regions are disordered phases with $[\eta(\mathbf{r})]^2$ close to 0.0. Therefore, the dark lines in Fig. 3 are antiphase domain boundaries. The morphologies generated show a remarkable similarity to experimental Transmission Electron Microscopy (TEM) observations in ordering systems.

The kinetics of ordering can also be characterized by the temporal evolution of the degree of order as measured by the average value of the long-range order parameter over all the lattice sites. This parameter is plotted in Fig. 4 as a function of reduced

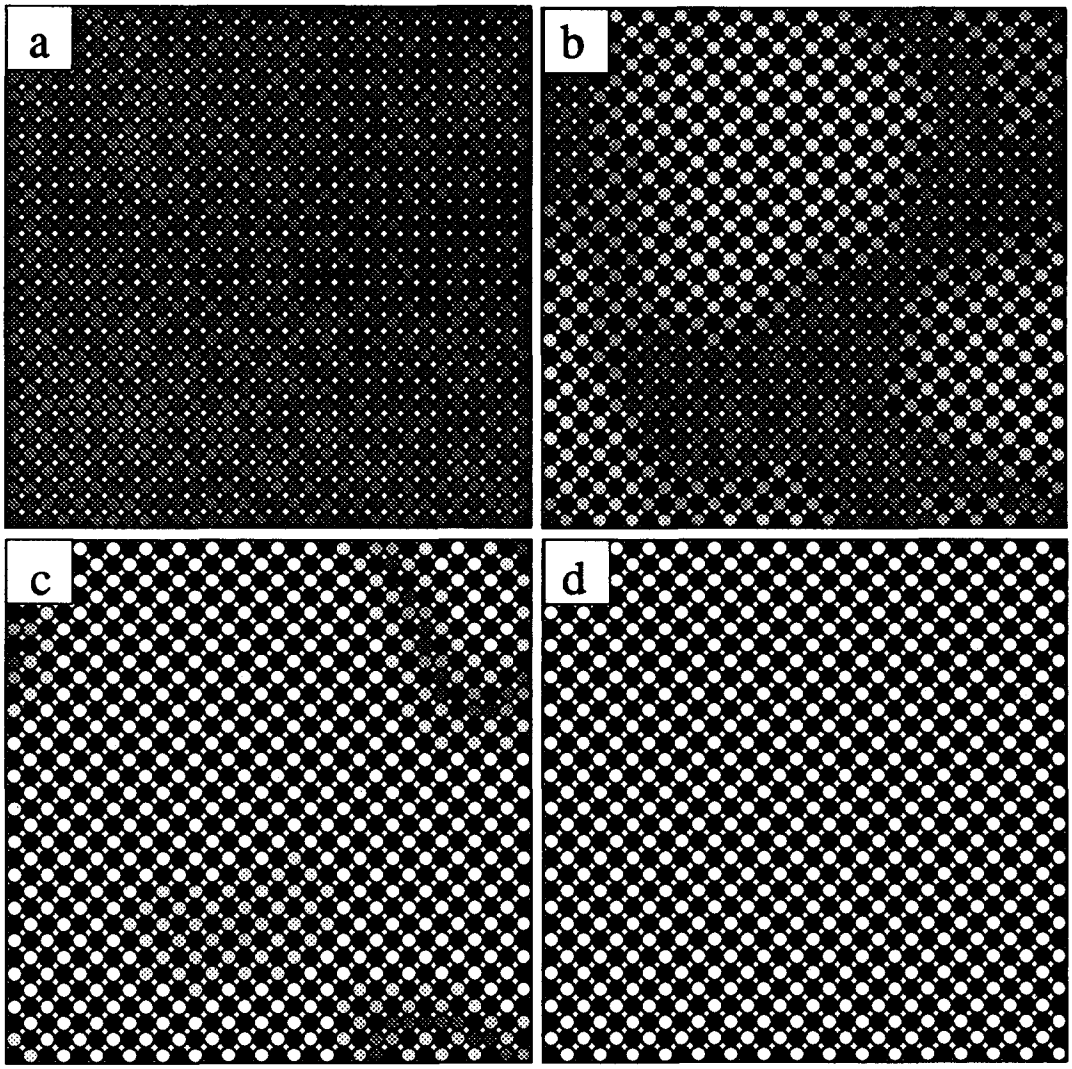


Fig. 2. Temporal evolution of the single-site distribution function at each lattice site for a computational cell of 32 × 32. The values of the single-site distribution function are represented by gray-levels with the completely black circles representing 1.0 and completely white circles representing 0.0. (a) $t^* = 0.0$; (b) $t^* = 1.5$; (c) $t^* = 2.0$; (d) $t^* = 10.0$.

time for different system sizes from a completely homogeneous system to a system with 256 × 256 lattice sites. It is seen that, regardless of system size, there is an incubation period of about 1 unit of reduced time before significant ordering occurs. Ordering occurs between reduced time $t^* = 1.0$ and

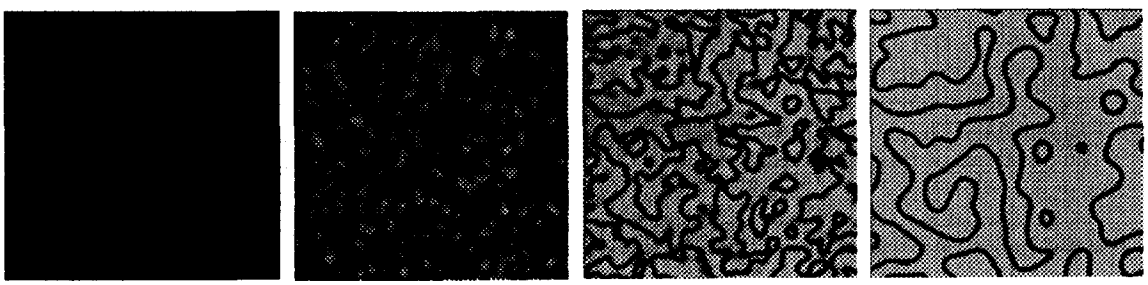


Fig. 3. Temporal evolution of square of the spatial long-range parameter distribution for a computational cell of 256 × 256. The values of the long-range order parameter are represented by gray-levels with the completely black representing 0.0 and completely white representing 1.0. (a) $t^* = 0.0$; (b) $t^* = 1.5$; (c) $t^* = 2.0$; (d) $t^* = 10.0$.

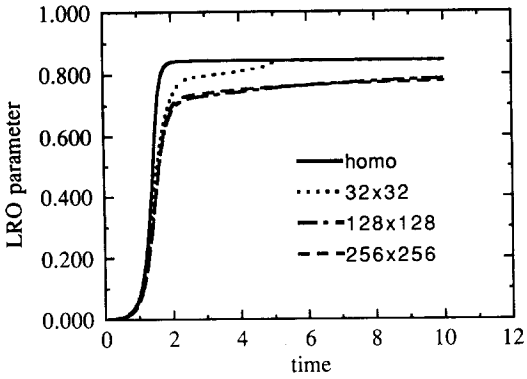


Fig. 4. The average long-range order parameter as a function of time for four systems with different system sizes.

$t^* = 2.0$. After $t^* = 2.0$, the evolution of single-site distribution functions corresponds to coalescence and coarsening of ordered domains. It is quite clear that even though the qualitative picture of the ordering kinetics is the same for all different system sizes, the $32 \times 32$ system size is insufficient if antiphase domain coarsening kinetics is to be investigated.

*Spinodal decomposition*

In this example, we also assume a nearest-neighbor interaction model. The bond energy values are taken to be

$$V^1_{AA} = -1.0, V^1_{BB} = -1.0, V^1_{AB} = -0.5. \quad (14)$$

The effective interchange energy $\epsilon_1$ calculated with these bond energies is negative, so phase separation is expected for a quenched disordered state. An average composition $c = 0.5$ and annealing temperature $0.5\ (\epsilon_1/k)$ are chosen for the study. The time step, $\Delta t$, is chosen to be 0.1. The initial state at $t^* = 0$ is generated in exactly the same way as in the ordering example.

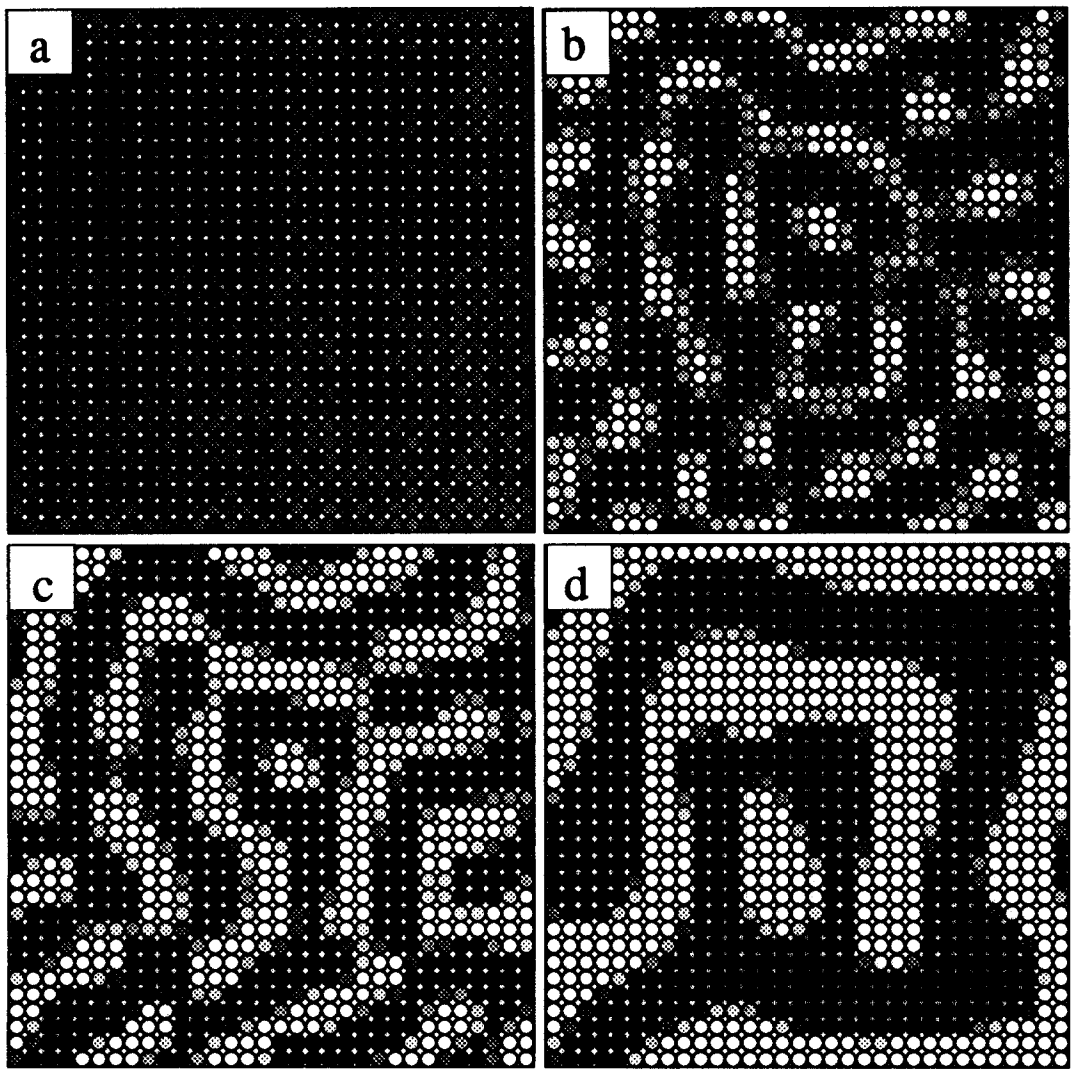


Fig. 5. Temporal evolution of the single-site distribution function at each lattice site for a computational cell of $32 \times 32$. The values of the single-site distribution function are represented by gray-levels with the completely black circles representing 1.0 and completely white circles representing 0.0. (a) $t^* = 0.05$; (b) $t^* = 4.0$; (c) $t^* = 10.0$; (d) $t^* = 200.0$.

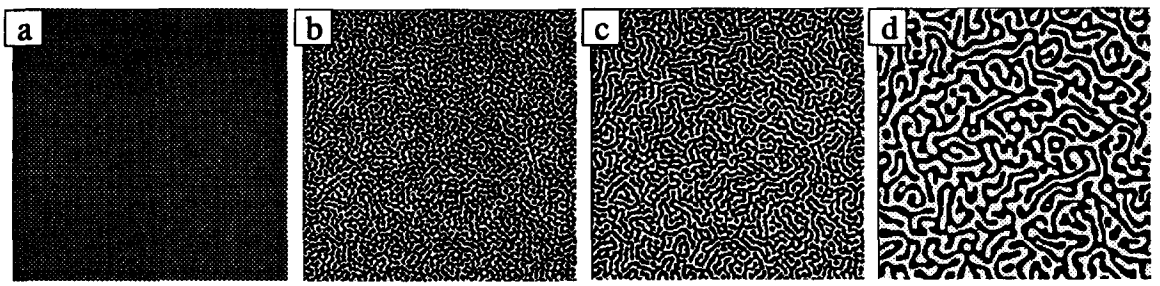


Fig. 6. Temporal evolution of the single-site distribution function at each lattice site for a computational cell of 256 × 256. The values of the single-site distribution function are represented by gray-levels with the completely black circles representing 1.0 and completely white circles representing 0.0. (a) $t^* = 0.05$; (b) $t^* = 4.0$; (c) $t^* = 10.0$; (d) $t^* = 200.0$.

The evolution of the single-site distribution function for a 32 × 32 computational cell is shown in Fig. 5. Figure 5(a) represents the initial disordered state which has an average composition 0.5 with random perturbations. Figure 5(b) shows the development and growth of A-rich and B-rich regions. At $t^* = 10$, the decomposition process is essentially completed. After $t^* = 10$, the morphological evolution corresponds to coarsening or Ostwald ripening.

The morphological evolution during a spinodal decomposition generated from a computer simulation with a larger system, 256 × 256, is shown in Fig. 6.

We can also define an order parameter for the case of spinodal phase separation, namely, the average value of $[c(\mathbf{r}) - c_0]$, where $c(\mathbf{r})$ is the local composition and $c_0$ is the average composition, over all the lattice sites. Three curves are plotted in Fig. 7 for system size 32 × 32, 128 × 128 and 256 × 256, respectively. At the temperature $0.5\frac{\epsilon_1}{k}$, it appears that a computational cell of 32 × 32 lattice sites produces essentially the same results as a system with 256 × 256 lattice sites. It starts with an incubation stage followed by decomposition and coarsening. Whether the system size is sufficient or not largely depends on the wavelength of the concentration domains which in turn depends on the annealing temperature and annealing time. A system size is reasonable as long as the wavelength of the composition domain is significantly smaller than the system size.

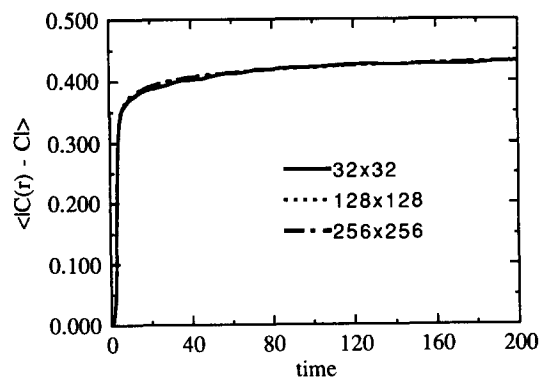


Fig. 7. The average deviation of local composition from the overall composition as a function of time for three systems with different system sizes.

*Simultaneous ordering and phase separation*

To produce simultaneous ordering and phase separation, interatomic interactions have to be extended at least into the second neighbor shell. We chose the following values for the bond energies

$$V^1_{AA} = 0.0, V^1_{BB} = 0.0, V^1_{AB} = 0.0$$
$$V^2_{AA} = 0.0, V^2_{BB} = 0.0, V^2_{AB} = 0.5. \qquad (15)$$

The equilibrium phases at the ground state derived from this set of parameters include pure A, pure B and an ordered phase AB with ordering wave-vector $(2\pi/a_0)$ $(\frac{1}{2},\frac{1}{2})$ where $a_0$ is the lattice parameter of the square lattice. Since we have presented no algorithm for determining the equilibrium phase diagram for the single-site approximation in cluster activation method, an equilibrium phase diagram derived from the true mean-field free energy is shown in Fig. 8 [3].

In the computer simulation, a disordered alloy with an average composition 0.25 is quenched to temperature 0.75 $(\epsilon_2/k)$ which is within the two-phase field of ordered and disordered phases and represented by a circle in the phase diagram. The time step $\Delta t$ is chosen

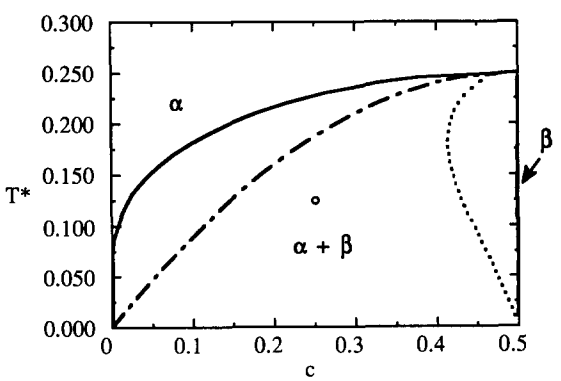


Fig. 8. The mean-field equilibrium phase diagram calculated with the set of energy parameters given in (12). $\alpha$ is the disordered phase and $\beta$ is the ordered phase. The solid line represents the equilibrium solvus line of the disordered phase. The solvus line for the ordered $\beta$ phase is almost vertical. The dot-dashed line is the order–disorder transition line and the dotted line is the conditional spinodal line [25].

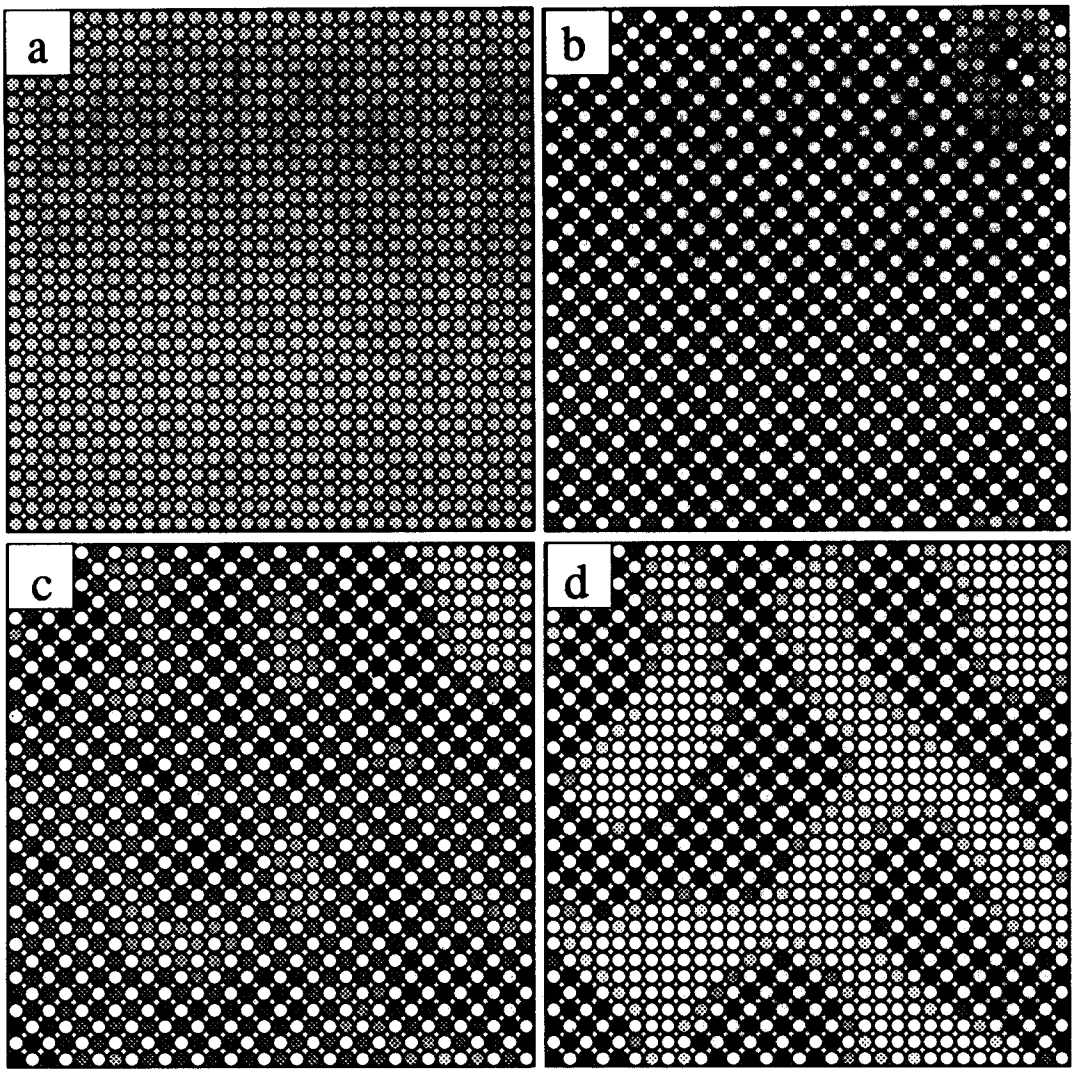


Fig. 9. Temporal evolution of the single-site distribution function at each lattice site for a computational cell of 32 × 32. The values of the single-site distribution function are represented by gray-levels with the completely black circles representing 1.0 and completely white circles representing 0.0. (a) $t^* = 0.05$; (b) $t^* = 1.5$; (c) $t^* = 10.0$; $t^* = 50.0$.

to be 0.1. The temporal evolution of the inhomogeneous single-site distribution function for a computational cell of 32 × 32 lattice sites is shown in Fig. 9. Similar to previous investigations of precipitation kinetics of ordered intermetallics using the Onsager-type microscopic diffusion equations [3], the first process during annealing of a disordered state below the ordering instability line but within the two-phase field of ordered and disordered phases is a congruent ordering after an incubation stage. The congruent ordering produces an ordered single-phase with antiphase domain boundaries [Fig. 9(b)]. However, this single-phase is unstable with respect to the subsequent decomposition into a two-phase mixture of ordered and disordered phases [Fig. 9(c, d)].

The morphological evolution of a larger computation cell, 256 × 256, is shown in Fig. 10 where the square of the long-range order parameter profiles is represented by gray-levels. Figure 10(a, b) represent the ordered domain nucleation and growth while Fig. 10(c, d) display the decomposition of the ordered single-phase. The decomposition is shown to start from the antiphase domain boundaries of the congruently ordered single-phase.

In systems with both ordering and phase separation, the kinetics may be described by two order parameters. One is the long-range order parameter as defined in the ordering example and the other is the compositional order parameter as defined in the spinodal decomposition example. Both parameters are plotted in Fig. 11 as function of time for a 32 × 32 system and a 256 × 256 system. Four stages of transformations are clearly seen for both system sizes. The period between $t^* = 0$ and 1.0 is the incubation stage; between $t^* = 1.0$ and 2.0 is the ordering stage; between $t^* = 2.0$ and 18.0 is the decomposition stage;

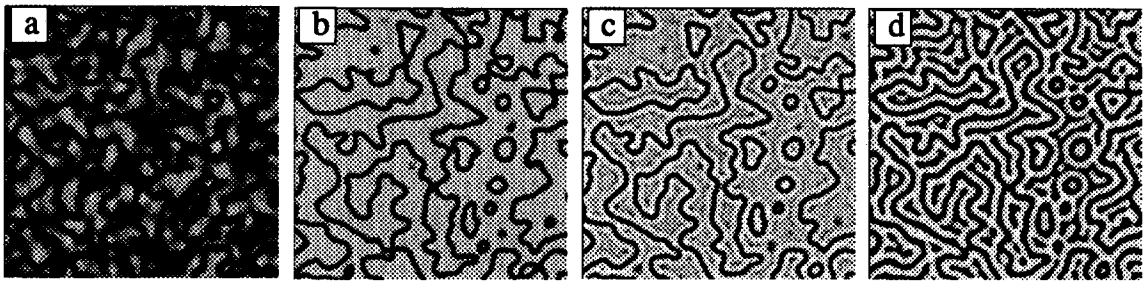


Fig. 10. Temporal evolution of square of the spatial long-range parameter distribution for a computational cell of 256 × 256. The values of the long-range order parameter are represented by gray-levels with the completely black representing 0.0 and completely white representing 1.0. (a) $t^* = 0.0$; (b) $t^* = 1.5$; (c) $t^* = 10.0$; (d) $t^* = 50.0$

and after $t^* = 18.0$ is the coarsening stage. It seems to be the case that the decomposition process is faster in the 256 × 256 system than the 32 × 32 system. By examining the morphologies for the two cases, it is quite obvious that the difference in the decomposition kinetics is due to the density of antiphase domain boundaries. For the 32 × 32 system, almost a single domain is formed before significant decomposition occurs because of antiphase domain coarsening and the small system size. It appears that the rate of decomposition of an ordered phase into a mixture of ordered and disordered phases is significantly enhanced by the existence of antiphase domain boundaries in the congruently ordered single-phase.

## DISCUSSION

Two of the major assumptions in the Onsager- and Langevin-type kinetic equations are the linear proportionality of the rate of change to the thermodynamic driving force and the constant value of the proportionality coefficient. Ludwig and Park compared the kinetics derived from the Langevin-type equations to kinetic Ising models with Monte-Carlo dynamics and thermally activated dynamics using a magnetic spin model [26]. They concluded that when the driving force is large, there are significant differences in the kinetics described by the Langevin equations and kinetic Ising models. The difference can be significantly reduced, however, in the small or intermediate-driving force regime if the proportionality constant is chosen to depend on the magnetization in a specific way. Recently, Martin [27] and Gouyet [28] showed that the proportionality constant or mobility term in the Cahn–Hilliard equation depends not only on local composition, but also on the local composition gradient.

By examining the long-range kinetics derived from the Onsager-type microscopic diffusion equations and that from the present cluster activation method, we also found significant differences not only in the ordering kinetics but also in the equilibrium state even though in both cases the single-site approximation is employed.

From Onsager-type diffusion theory using a mean-field free energy, the kinetic equation of homogeneous order for the ordered phase described in the ordering example is given by

$$\frac{d\eta}{dt} = -L\left\{\frac{2\epsilon_1\eta}{kT} + \ln\left(\frac{1+\eta}{1-\eta}\right)\right\} \qquad (16)$$

where $\eta$ is the long-range order parameter, $\epsilon_1$ is the nearest neighbor interchange energy given in (11) and $L$ is the probability of atomic interchange within a time unit. The kinetic equation of homogeneous

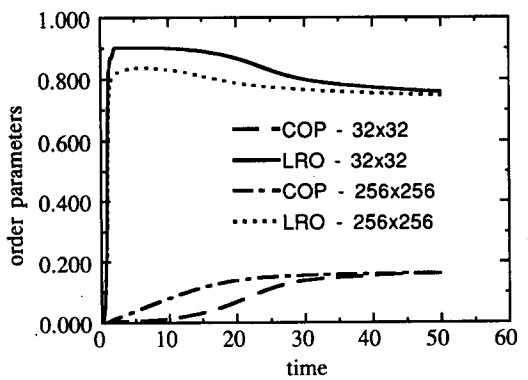


Fig. 11. Average long-range order parameter and average deviation of local composition from the overall composition as functions of time for two systems with different system sizes.

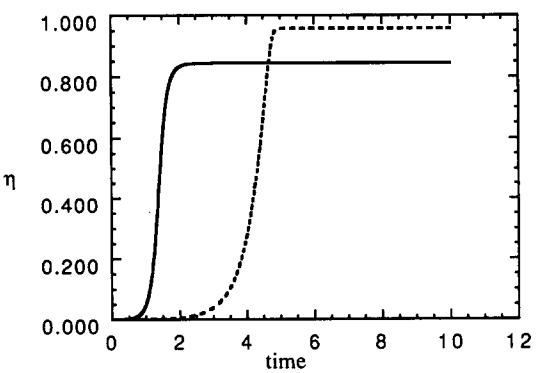


Fig. 12. Long-range order parameter as a function of time derived from the Onsager-type microscopic diffusion equation (the dotted line) and the cluster activation method in the single-site approximation (the solid line).

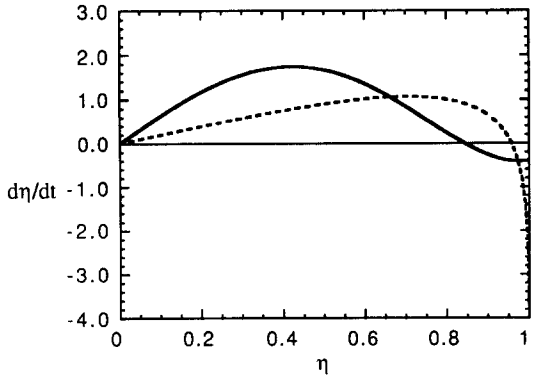


Fig. 13. The rate, $d\eta/dt$, as a function of $\eta$ for the two kinetic models. Dotted line—the Onsager-type microscopic diffusion equation; solid line—the cluster activation method in the single-site approximation.

order for the same ordered phase from cluster activation method is given by Vineyard [8]

$$\frac{d\eta}{dt} = \frac{1}{2}K_0(1-\eta)^2 - \frac{1}{2}K_d(1+\eta)^2 \qquad (17)$$

where $K_0$ and $K_d$ are given by

$$K_d = 4.0\nu \exp\left(-\frac{U_0}{kT}\right)\exp\left(\frac{3\epsilon_1}{2kT}\right) \times \left\{1+\frac{1}{2}\left(1+\eta\right)\left[\exp\left(-\frac{\epsilon_1}{3kT}\right)-1\right]\right\}^6$$

$$K_0 = 4.0\nu \exp\left(-\frac{U_0}{kT}\right)\exp\left(-\frac{3\epsilon_1}{2kT}\right) \times \left\{1+\frac{1}{2}(1+\eta)\left[\exp\left(\frac{\epsilon_1}{2kT}\right)-1\right]\right\}^6.$$

We assume that

$$\exp\left(-\frac{U_0}{kT}\right)$$

corresponds to $L$ in equation (16) since both of them are interchange probabilities per unit time. The time dependence of long-range parameter $\eta$ from the two kinetic equations are given in Fig. 12 for a temperature $0.5\,\epsilon_1/k$. It is shown that ordering kinetics from the two different equations are quite different. Ordering occurs at an earlier time in the cluster activation equation than the Onsager-type equation. Moreover, the ordering occurs faster in cluster activation method than that described by Onsager-type equation. This difference can also be clearly seen in the plot of the rate of long-range development as a function of long-range order parameter as shown in Fig. 13 for both kinetic models.

Only those order parameters which correspond to a positive value of $d\eta/dt$ in Fig. 13 can grow. The interception of $d\eta/dt$ with the line $d\eta/dt = 0$ gives the equilibrium long-range order parameter values ($d\eta/dt = 0$ at $\eta = 0$ corresponds to the unstable solution). It is apparent from Figs 12 and 13 that the equilibrium values of the long-range order parameter at the same temperature $0.5\,\epsilon_1/k$ are considerably different. The equilibrium solution for homogeneous order in the single-site approximation in cluster activation method has been derived by Yamauchi who also compared the results with the Bethe and Bragg–Williams approximation [29].

The equilibrium long-range order parameter derived from the condition $d\eta/dt = 0$ in equation (17) is given by

$$\eta_{eq} = \frac{1-\frac{1}{8}\exp\left(\frac{3\epsilon_1}{2kT}\right)\left\{1-\sqrt{1-4\exp\left(-\frac{\epsilon_1}{kT}\right)}\right\}^3}{1+\frac{1}{8}\exp\left(\frac{3\epsilon_1}{2kT}\right)\left\{1-\sqrt{1-4\exp\left(-\frac{\epsilon_1}{kT}\right)}\right\}^3}. \qquad (18)$$

The critical temperature for ordering, $T_c$, is determined by the condition that the term inside the square-root is zero, i.e.

$$1-4\exp\left(-\frac{\epsilon_1}{kT_c}\right)=0. \qquad (19)$$

An approximate value of 0.72135 is obtained for $T_c$ with $\frac{\epsilon_1}{k} = 1.0$. This is exactly the same value for critical temperature that one would obtain from the Bethe approximation in which

$$T_c = \frac{\epsilon_1}{2k\ln\left(\frac{z}{z-2}\right)} \qquad (20)$$

where $z$ is the coordination number which is 4 in the case of square lattice. The critical temperature in the Bragg–Williams approximation is

$$T_c = \frac{\epsilon_1}{k}. \qquad (21)$$

A plot of the equilibrium long-range order parameter as a function of temperature in cluster activation method from equation (18) together those

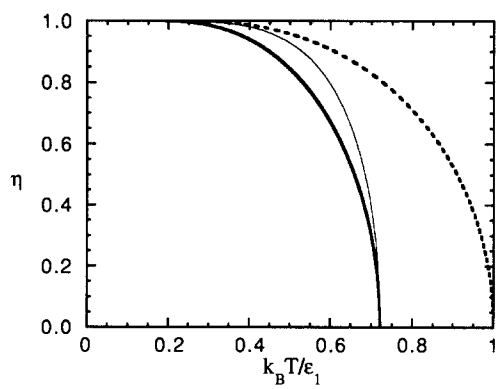


Fig. 14. Equilibrium long-range order parameter as a function of temperature derived from cluster activation method in the single-site approximation (the thick solid line), the Bethe approximation (the thin solid line) and the Bragg–Williams approximation (the dotted line).

derived from the Bethe and Bragg–Williams approximation shows that the single-site approximation in cluster activation method produces equilibrium states much closer to the Bethe approximation than the Bragg–Williams approximation (Fig. 14). However, the equilibrium states derived from the single-site approximation in cluster activation method are not exactly the same as the Bethe approximation as one would expect.

The reason that the equilibrium states derived from the single-site approximation of cluster activation method are different from the B–W approximation is due to the fact that in cluster activation method, the nearest neighbor pairs have to be considered for the atomic interchange, which is not consistent with the B–W approximation in which a single-site is considered. For example, the number of bonds which are broken around a given point during an atomic exchange is three in a two-dimensional square lattice in the cluster activation method description whereas it is four in the B–W approximation. Therefore, the transition temperature obtained from cluster activation method in a nearest-neighbor interaction model will be approximately $(z-1)/z$ times the transition temperature obtained from a true single-site mean-field model. However, the configuration entropy description in the single-site approximation of the cluster activation method is different from the pair approximation. As a result, even though the critical temperature in the single-site approximation of cluster activation method is the same as the Bethe's approximation, the dependence of the equilibrium order on temperature is not.

## SUMMARY

A simple computer simulation technique applying the microscopic master equations to diffusional phase transformations has been exhibited. It can successfully describe ordered domain nucleation and growth, antiphase domain coarsening, compositional phase separation, Ostwald ripening, and simultaneous ordering and phase separation. It is shown that annealing of a disordered phase within a single-phase field of an ordered phase in a phase diagram goes through three stages of transformations which include incubation, homogeneous nucleation and growth of ordered domains, and domain coalescence and coarsening. In the case of spinodal decomposition, the three stages are incubation, decomposition and Ostwald ripening. Annealing of a quenched alloy below a tricritical point of a phase diagram results in four stages which are incubation, ordering, decomposition and Ostwald ripening. It is demonstrated that the antiphase domain boundaries formed at the ordering stage speed up the subsequent decomposition process significantly.

The present technique assumes a direct exchange mechanism for atomic diffusion and a single-point probability approximation for the description of structural states. Nonetheless, the single-site approximation in this kinetic model produces a thermodynamic description closer to the Bethe than the Bragg–Williams approximation. Computer simulation of diffusional transformations using a vacancy mechanism and higher order clusters will be described in future publications.

*Acknowledgements*—This work is supported by the ARPA/NIST Program on Mathematical Modeling of Microstructure Evolution in Advanced Alloys and by NSF under the grant number DMR-9311898. We are very grateful to Fannie Mui who did most of the computer programming work. We also thank Drs John Cahn at NIST and R. Kikuchi at UCLA for enlightening discussions.

## REFERENCES

1. For a review, see J. D. Gunton, M. San Miguel and P. S. Sahni, in *Phase Transitions and Critical Phenomena* (Edited by J. Lebowitz), Vol. 8, p. 267. Academic Press, London (1983).
2. A. G. Khachaturyan, *Sov. Phys. Solid State* **9,** 2040 (1968).
3. L. Q. Chen and A. G. Khachaturyan, *Acta metall. mater.* **39,** 2533 (1991); *Phys. Rev. Lett.* **70,** 1477 (1993).
4. L. Q. Chen and A. G. Khachaturyan, *Phys. Rev. B* **46,** 5899 (1992); **44,** 4681 (1991).
5. Y. Z. Wang, L. Q. Chen and A. G. Khachaturyan, *Acta metall. mater.* **41,** 279 (1992).
6. L. Q. Chen, Y. Z. Wang and A. G. Khachaturyan, *Phil. Mag. Lett.* **65,** 15 (1992); **64,** 241 (1991).
7. J. A. Simmons and L. Q. Chen, to be published.
8. G. H. Vineyard, *Phys. Rev.* **102,** 981 (1956).
9. L. Q. Chen, *Phys. Rev. B* **49,** 3791 (1994).
10. F. Ducastelle, *Prog. Theoret. Phys. Suppl.* To be published.
11. R. Kikuchi, *Ann. Phys.* **10,** 127 (1960); *Prog. Theor. Phys.* Suppl. **35,** 1 (1969).
12. K. Gschwend, H. Sato and R. Kikuchi, *J. Phys. (Paris)* **C7,** 357 (1977); *J. Chem. Phys.* **69,** 5006 (1978); **71,** 2844 (1979).
13. H. Sato and R. Kikuchi, *Acta metall.* **24,** 797 (1976).
14. S. Iida, *J. Phys. Soc. Japan* **10,** 769 (1955).
15. B. W. Roberts and G. H. Vineyard, *J. appl. Phys.* **27,** 203 (1956).
16. I. I. Kidin and M. A. Shtemel, *Fiz. metal. metalloved.* **11,** 641 (1961).
17. D. O. Welch, *Mat. Sci. Engng* **4,** 9 (1969).
18. S. Radelaar, *J. Phys. Chem. Solids* **31,** 219 (1970).
19. H. Yamauchi and D. de Fontaine, in *Order–Disorder Transformations in Alloys* (edited by H. Warlimont), p. 148, Springer, Berlin (1974).
20. C. M. Van Baal, *Physica A* **111,** 591 (1982); C. M. Van Baal, *Physica A* **113,** 117 (1982); *Physica A* **196,** 116 (1993).
21. A. S. Bakai and M. P. Fateev, *Physica status solidi* (b) **158,** 81 (1990).
22. L. Anthony and B. Fultz, *J. Mater. Res.* **4,** 1132 (1989).
23. B. Fultz, *Acta metall.* **37,** 823 (1989); *J. Mater. Res.* **5,** 1419 (1990).
24. C. M. Van Baal, *Physica A* **129,** 601 (1985).
25. S. M. Allen and J. W. Cahn, *Acta metall.* **24,** 425 (1976).
26. K. F. Ludwig Jr and B. Park, *Phys. Rev. B* **46,** 5079 (1992).
27. G. Martin, *Phys. Rev. B* **41,** 2279 (1990).
28. J.-F. Gouyet, *Europhys. Lett.* **21,** 335 (1993).
29. H. Yamauchi, *Scripta metall.* **7,** 109 (1973).